Biophysical Journal
Article

Biophysical Society

Subharmonics and Chaos in Simple Periodically Forced Biomolecular Models

Evgeni V. Nikolaev,[1] Sahand Jamal Rahi,[2] and Eduardo D. Sontag[1,3,*]
[1]Center for Quantitative Biology, Rutgers University, Piscataway, New Jersey; [2]Department of Physics and Center for Brain Science, Harvard University, Cambridge, Massachusetts; and [3]Department of Electrical and Computer Engineering and Department of Bioengineering, Northeastern University, Boston, Massachusetts

ABSTRACT This article uncovers a remarkable behavior in two biochemical systems that commonly appear as components of signal transduction pathways in systems biology. These systems have globally attracting steady states when unforced, so they might have been considered uninteresting from a dynamical standpoint. However, when subject to a periodic excitation, strange attractors arise via a period-doubling cascade. Quantitative analyses of the corresponding discrete chaotic trajectories are conducted numerically by computing largest Lyapunov exponents, power spectra, and autocorrelation functions. To gain insight into the geometry of the strange attractors, the phase portraits of the corresponding iterated maps are interpreted as scatter plots for which marginal distributions are additionally evaluated. The lack of entrainment to external oscillations, in even the simplest biochemical networks, represents a level of additional complexity in molecular biology, which has previously been insufficiently recognized but is plausibly biologically important.

INTRODUCTION

Many unforced biochemical systems, such as pairs of mutually repressing genes, or phosphorylation/dephosphorylation cycles, can exhibit biologically important properties such as multistability and oscillations (1–8). The experimental observation of these behaviors helps one to distinguish among alternative models, and indicates the necessity of positive or negative feedback loops (9). Biological observables exhibited in response to time-dependent forcing signals (i.e., dynamic phenotypes) can provide further insight into the structure of biological systems. Recent examples include scale invariance or "fold-change detection" (10–12), nonmonotonic behavior under monotonic inputs (13), refractory period stabilization (14), and nonentrained solutions or "period skipping" when stimuli are periodic (14).

The goal of Rahi et al. (14) was to find tools that allow one to distinguish between different perfect adaptation topologies. It is known that adaptation requires the existence of incoherent feedforward or negative feedback subnetworks. Either of these works, giving asymptotically the same behavior under constant stimulation. On the other hand, responses to nonconstant inputs allow a finer model discrimination. Indeed, it is shown theoretically in (14) that both feedforward loops and positive feedback loops can never destroy entrainment, leaving negative feedback as the only explanation for lack thereof. Rahi et al. (14) found experimentally, in a *Caenorhabditis elegans* odor-sensing neuron, responses whose periods are roughly multiples of the period T of an excitation signal, thus theoretically implying the presence of negative feedback loops, and went on to propose a circuit architecture that is capable of displaying the observed dynamic phenotype. These findings suggest the following theoretical question: what complicated dynamics can arise in the simplest biochemical systems, more generally, in response to a periodic input? Here we answer that question by showing that a negative feedback system motivated by (14), and also the "nonlinear integral feedback" circuit proposed in (10) for scale-invariance, can both exhibit a rich bifurcation structure and chaotic behavior in response to pulse-train excitations.

There is an extensive and deep literature that deals with the analysis of responses of nonlinear systems, and particularly oscillators, to periodic signals. Under the influence of external periodic environmental forcing, nonlinear systems can exhibit bifurcations leading to subharmonic responses and chaos. Such behaviors have been studied theoretically and experimentally, in squid axons (15), cellular circadian oscillations subjected to periodic forcing by a light-dark cycle (16), forced pendulums and other classical physical

Submitted August 9, 2017, and accepted for publication January 8, 2018.
*Correspondence: eduardo.sontag@gmail.com
Editor: Fazoil Ataullakhanov.
https://doi.org/10.1016/j.bpj.2018.01.006

oscillators described by the van der Pol and the Duffing equations (17–23), and biochemical oscillators such as the "Brusselator" (24,25). Our contribution is to show that similar behaviors can be found already in two of the simplest nonlinear systems, which appear in the current systems biology literature. Furthermore, and perhaps equally remarkable, our two systems are not rhythmic in the absence of periodic stimulation; quite the contrary, they have unique and globally asymptotically stable steady states when the input is constant. This complexity in ubiquitous systems that constitute components of typical signal sensing and transduction networks suggests a previously unrecognized hidden level of complexity in molecular biology, which is of significance for biological function (14).

MATERIALS AND METHODS

We first discuss the models to be considered, the type of periodic input, and the notion of chaos.

The two models

Our first example, motivated by (14), where similar models appear, is a negative feedback system that consists of two species X and Y such that X enhances the production of Y and Y inhibits the production of X. The concentrations of X and Y at time t are denoted respectively by $x = x(t)$ and $y = y(t)$. The interaction terms are modeled by Michaelis-Menten kinetics, and both X and Y are subject to zeroth-order decay through a mechanism such as protease-mediated degradation. An external input U, with magnitude $u = u(t)$ in appropriate units, triggers production of X. The equations are as follows:

$$\frac{dx}{dt} = \frac{\sigma_x u(t)}{\theta_y + y} - \frac{\mu_x x}{M_x + x}, \tag{1a}$$

$$\frac{dy}{dt} = \frac{\sigma_y x}{\theta_x + x} - \frac{\mu_y y}{M_y + y}, \tag{1b}$$

where we omit the argument t in x and in y, but leave it in the input to emphasize its time-dependence. All constants are assumed to be positive. A diagram of this model is in Fig. 1, *a* and *c*, with a general periodic input or a pulsed input, respectively.

To emphasize that the bifurcation behaviors are not an artifact of artificially chosen parameter values, we will also consider the special case of model 1 in which all parameter values are unity ($\sigma_x = \sigma_y = \theta_x = \theta_y = \mu_x = \mu_x = M_x = M_y = 1$). We call this the "unity" model.

Our second example originates in (10) (see (26) for more theoretical analysis). It is an integral feedback system consisting of a regulator species X and an output species Y, with equations (using again x, y, and u for concentrations and inputs) as follows:

$$\frac{dx}{dt} = ax(y - y_0), \tag{2a}$$

$$\frac{dy}{dt} = \frac{cu(t)}{K_x + x} - dy. \tag{2b}$$

In model 2, $a = Y_0 = c = d = 1.0$. Thus, model 2 is also a unity model. We use a small (nonzero) parameter K_x, $0 < K_x << 1$, for the sake of computational feasibility only to avoid division by zero or very small numbers. For a Michaelis-Menten constant K_x, $0 < K_x << 1$, this system is perfectly adapting to constant inputs and has the scale invariance or fold-change detection property, as discussed in (10). A diagram of this model is in Fig. 1, *b* and *d*, with a general periodic input or a pulsed input, respectively.

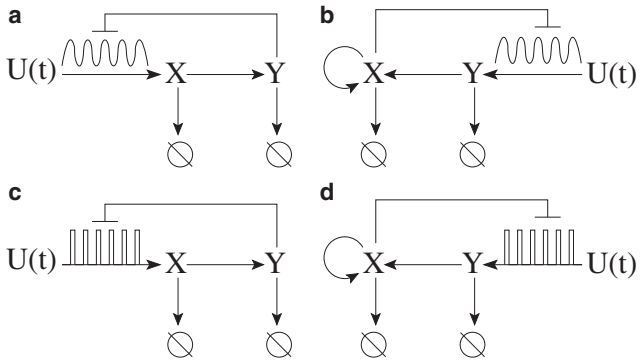

FIGURE 1 Simple biocircuits with an arbitrary periodic input and a negative feedback output. (*a* and *c*) Negative feedback system. (*b* and *d*) Fold-change detection system. (*a* and *b*) Arbitrary periodic input. (*c* and *d*) Pulse train input.

Both examples have the property that when $u(t)$ is a constant there cannot be any periodic orbits and, furthermore, all solutions converge to a globally asymptotically stable steady state (with one minor exception for model 1, explained in the Supporting Material, which arises when some solutions become unbounded). For the system defined by model 2, this fact was proved in (26). For the system described by model 1, this is discussed in the Supporting Material.

Inputs

For simplicity, and to connect with the experiments in (14), we will consider T-periodic input functions $u(t)$ (i.e., $u(t) \equiv u(t + T)$), which consist of pulse trains of period T:

$$u(t) = \begin{cases} 0, & 0 \le t < t_1, \\ m, & t_1 \le t < t_2, \\ 0, & t_2 \le t \le T. \end{cases} \tag{3}$$

In Eq. 3, $t_1 = (T - \Delta)/2$, $t_2 = (T + \Delta)/2$, where T and Δ are the period and support of the input function $u(t)$, respectively. For the sake of (computational) simplicity, the support interval, $[t_1,t_2]$, is centered at the midpoint of the interval $[0,T]$. We will analyze the effects of different choices of the amplitude parameter m or period T.

Chaos

There are many definitions of chaos, the choice of which depends on the aspect of chaos to be emphasized (22,27–32).

The definition of chaos appropriate for our work is based on periodic orbits and corresponds to the transition to chaos though period-doubling cascades (33–35). Following (35), we say that the given dynamic system has a periodic-orbit chaos or a periodic orbit strange attractor, if it has infinitely many regular periodic saddles.

Specifically, in the context of this work we reduce the bifurcation analysis of our models to the bifurcation analysis of the corresponding period-T maps Φ of the plane, Φ: $\mathbb{R}^2 \to \mathbb{R}^2$. In this case, periodic solutions of the models, of period kT, are in one-to-one correspondence with the respective fixed points of Φ^k, $k - 1$,.... We call a k-periodic orbit $\{z_0, \ldots, z_{k-1}\}$ of the map Φ a regular saddle periodic orbit or a regular periodic

saddle, $z_{n+1} = \Phi(z_n)$, $n = 0, \ldots, k-1$, with $z_k = \Phi(z_0)$ if the Jacobian matrix $\partial\Phi^k(z_0)/\partial z$ has two eigenvalues $|\mu_1| < 1$ and $|\mu_2| > 1$.

It is instructive to compare our biocircuit models with the Duffing's equation, the second-order ordinary differential equation (ODE) with a cubic nonlinearity describing a driven damped anharmonic oscillator, $x'' + kx' + x^3 = B\cos\omega t$. Here, the parameter k controls the damping, and the parameter B controls the amplitude of an external periodically varying driving force (17,22). Chaotic solutions of the Duffing's equation were discovered as early as 1962–63 (20,21,23) and have been the subject of extensive research (18,34,36). Detailed reviews of the Duffing equation's fundamental properties can be found in (22,32). In the examples studied below, a strange attractor emerges via a cascade of period-doubling bifurcations (35), the transition to chaos also observed in the Duffing's equation (34).

As already explained, when our biocircuits are subject to constant inputs, they admit a globally asymptotically stable state. However, when the external periodic force is allowed to act during a short period of time, very small relative to the period T, chaotic behavior emerges (Fig. 2). This phenomenon is discussed in detail throughout the rest of the article.

We conclude this section with a few qualitative motivating remarks. Specifically, although we focus on very simple and concrete examples of mathematical models manifesting complex chaotic dynamics, the models are analyzed in the constructive style of the modern theory of dynamical systems. Despite the fact that this mathematical theory is still complex, it has evolved to a point where it can be used to predict or, at least to motivate, both the existence and structure of complex dynamics in a systematic manner. We illustrate this next through two theoretical approaches.

First of all, by appending a third equation, $d\theta/dt = \omega$ with $\omega = 2\pi/T$, to the above-formulated 2D models, followed by an appropriate Fourier series approximation of the discontinuous 2π-periodic input function $v(\theta) = u(\theta.2\pi)$ to fulfill formal smoothness conditions, the extended approximated models can be viewed as a forced relaxation oscillator in the style of (30). Intuitively, as the steady state of our simple models depends on the input-level, if these input-levels oscillate, then the overall system's response is periodic and what we have is a relaxation oscillator. The theory developed by Guckenheimer et al. (30) predicts that this class of forced relaxation oscillators can have a positive measure set of parameter values for which trajectories with positive Lyapunov exponents exist.

Second, the approach developed by Sander and Yorke (35) provides insight into the origin of the chaotic dynamics studied below via period-doubling cascades.

Shift maps by period T

The piecewise definition given in Eq. 3 of the input $u(t)$ makes it inconvenient to numerically study bifurcations of limit cycles with respect to model parameters. It is more convenient to study the corresponding 2D-iterated maps, or shift maps by period T,

$$z_{n+1} = \Phi(z_n, \alpha), \quad z \in \mathbb{R}^2, \tag{4}$$

where $\Phi(z_n,\alpha)$ is the shift map by period T along the trajectories of the nonautonomous ODE given by Eqs. 1 or 2, respectively (recall that T is the (minimal) period of the external input $u(t)$). More precisely, we define $\Phi(z,\alpha) = \varphi^T(z,\alpha)$, where $\varphi^t(z,\alpha)$ is the solution of the given ODE, that is, $\varphi^t(z,\alpha) = (x(t,\alpha), y(t,\alpha))$, with the initial condition $z = (x,y)$ at $t = 0$. Equation 4 gives the value of z_{n+1} as a function of z_n ($n = 0,1,2,\ldots$), and α is the vector of model parameters. Note that a fixed point in Eq. 4 corresponds to the appropriate periodic solution of the ODE model considered.

Theoretical homotopy continuation (35) and numerical bifurcation approaches (37,38), as implemented for instance in the powerful numerical bifurcation tool MatcontM (38), can then be applied to study numerically bifurcations of fixed and periodic points of the iterated map $\Phi(z,\alpha)$ defined in Eq. 4. A technical requirement for these methods is that the map $\Phi(z,\alpha)$ should be smooth with respect to state variable z and parameter α. This requirement is easy to verify; see the Supporting Material.

RESULTS AND DISCUSSION

Off-on-off chaos

Numerical analysis of the discrete trajectories in Eq. 4 corresponding to the models described in the Supporting Material immediately reveals chaotic dynamics in a wide range of model parameters.

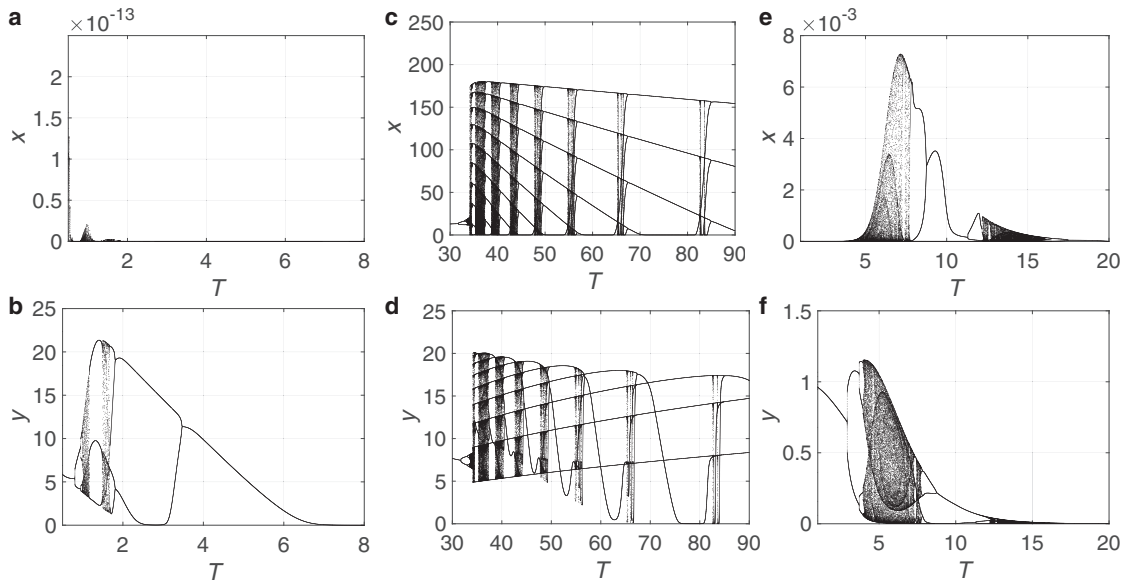

FIGURE 2 Bifurcation diagrams with respect to the external period T. Here, (*a*) and (*b*) correspond to model 1; (*c*) and (*d*) correspond to unity model 1; and (*e*) and (*f*) correspond to model 2.

Specifically, Fig. 2 demonstrates examples of bifurcation diagrams, when the values of the external period T are allowed to vary: 1) Fig. 2, *a* and *b*, corresponds to a strange attractor of the map in Eq. 4 for model 1 used with the fixed parameter values $\sigma_x = \sigma_y = 10^4$, $\theta_x = 10$, $\theta_y = 1$, $\mu_x = 100$, $\mu_y = 10$, $M_x = M_y = 1$, $m = 1.75$, and $\Delta = 10^{-4}$; 2) Fig. 2, *c* and *d*, corresponds to the map in Eq. 4 for the unity model 1 (with all parameters = 1) used with $m = 2.0 \times 10^4$ and $\Delta = 10^{-2}$; and 3) Fig. 2, *e* and *f*, corresponds to a strange attractor of the map in Eq. 4 for model 2 used with $m = 10^{-5}$, and $\Delta = 0.2$.

We observe from Fig. 2 that for large values of the external period T (that is, low frequencies, $\omega \to 0$), the dynamics in all the three models is asymptotically localized to a small vicinity of the unique globally stable steady state, corresponding to oscillations with a very small amplitude. Indeed, large periods of external forcing allow the dynamics systems to relax to their globally stable steady states.

However, as soon as the period T of the external input decreases, small amplitude oscillations develop into large-amplitude oscillations, followed by the transition to chaos via a period-doubling cascade. Remarkably, and counterintuitively, whereas the period T of the external input decreases, the period of periodic processes described by each periodically forced model increases before each model becomes fully chaotic.

If the external period T is further decreased, the chaotic dynamics is eliminated and is replaced again by regular periodic oscillations with period T. This backward transition, chaos $\to$ periodic oscillations, can be explained by the Krylov-Bogoliubov-Mitropolsky asymptotic theory (39,40). The theory predicts that asymptotically in the limit $\omega \to \infty$, the system dynamics becomes periodic with vanishing amplitude of oscillations. In this case, the high-frequency small-amplitude periodic dynamics can be approximated by a steady state in the corresponding autonomous (averaged) system (41).

The strange attractors shown in Fig. 2 are called "off-on-off" attractors (35), because the chaotic dynamics disappears for small and large values of the bifurcation parameter, period T in this case, and exists only for intermediate values of the parameter. Examples of chaotic time-resolved solutions for the strange attractors (Fig. 2) with positive largest Lyapunov exponents ($\lambda_{max} > 0$) (42), are shown in Fig. S3.1.

To gain additional insight into the geometry of the strange attractors corresponding to the bifurcations trees (Fig. 2) and their complex time-resolved realizations (Fig. S3.1), we then plotted their respective phase portraits for appropriate iterated maps from Eq. 4 as discussed earlier. In the case of discrete trajectories generated by the map in Eq. 4, it is convenient to interpret the phase portraits as scatter plots for which marginal distributions can be computed (see the Supporting Material). We observe from Figs. S4.1 and S4.3 that for model 1 with the parameters shown, and also for model 2, the discrete trajectories are localized along the axis *y*, respectively. However, in the special case of the unity model, the discrete trajectories stochastically jump between and stochastically move along several attractor loci (Fig. S4.1).

When instead of the external period T, the strength, m, or support, Δ, of the external input, are taken as bifurcation

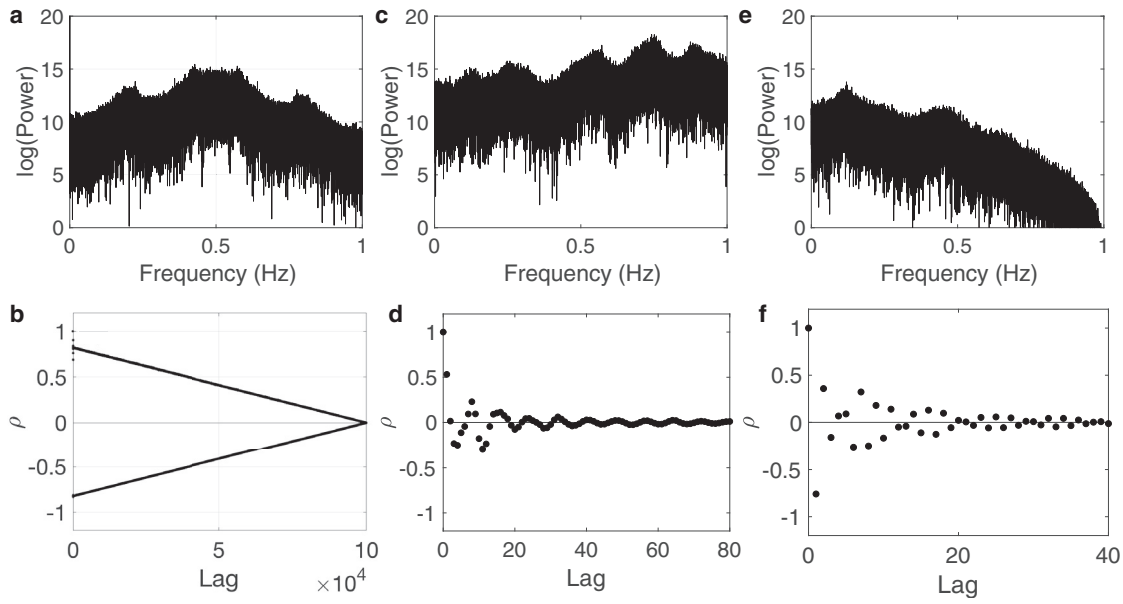

FIGURE 3 Power spectra and autocorrelation functions. Power spectra and ACFs are generated from the discrete chaotic trajectories of the corresponding iterated maps. Here, (*a*) and (*b*) correspond to the map in Eq. 4 for model 1 with period $T = 1$; (*c*) and (*d*) correspond to the map in Eq. 4 for the unity model with period $T = 40$; and (*e*) and (*f*) correspond to the map in Eq. 4 for model 2 with period $T = 5$.

parameters, similar results can be obtained (Figs. 5 and 6 and S5.1, respectively).

Power spectra and autocorrelation functions

In the theory of chaotic dynamic systems and discrete iterated maps (43), the power spectrum is computed and used to distinguish periodic, quasiperiodic, and chaotic motions described by dynamical systems arising in a broad range of fields (31). The power spectrum plotted for periodic or quasiperiodic trajectories has discrete peaks at the harmonic and subharmonics, whereas chaotic trajectories have a broadband component in their power spectrum. To illustrate that phenomenon for chaotic discrete trajectories of the iterated maps given in Eq. 4, we compute the power spectra and autocorrelation functions for the discrete trajectories corresponding to those values of parameters for which the plots in Fig. 2 (and Fig. S3.1) are obtained. To compute the power spectra and autocorrelation function (ACF), we use fast Fourier transform and ACF functions available from MATLAB (The MathWorks, Natick, MA) with $N_0 = 10^5$, the number of points used to compute both the power spectra and ACFs (Fig. 3).

Recall that the ACF $\rho(L)$ is defined and computed as follows (44):

$$\rho(L) = \lim_{N\to\infty} \frac{1}{N} \sum_{n=0}^{N} y_n\, y_{n-L} \approx \frac{1}{N_0} \sum_{n=0}^{N_0} y_n\, y_{n-L}. \qquad (5)$$

Here, N_0 is a sufficiently large integer, the integer argument L is called a lag (31,44), and y_n is, for example, the y component of the iterated phase point z_n, $z_n = (x_n, y_n)$, $z_n = \Phi(z_{n-1})$, $n = 1,2,\ldots$ (see the Supporting Material).

We also recall briefly that chaotic dynamics implies mixing and, therefore, a positive Kolmogorov entropy (31). As a result of the mixing effect, $\rho(L)$ decreases to zero exponentially at a rate determined by the Kolmogorov entropy (45).

We observe from Fig. 3 that the ACF in the case of model 1 converges to zero slowly, rapidly oscillating between positive and negative values, Fig. 3, *a* and *b*, whereas the ACF in both case of the unity model, Fig. 3, *c* and *d*, and model 2, Fig. 3, *e* and *f*, vanishes rapidly. This observation could be interpreted as saying that model 1 has a larger capacity for memory than the other two models in terms of its remembrance of the past.

Myrberg-Feigenbaum cascades

We continue our discussion of the bifurcation diagrams (Fig. 2) by analyzing the corresponding period-doubling cascades as discussed informally below. A rigorous definition of period-doubling cascades can be found in (33,35).

To begin with, we note that Pekka Myrberg, a Finnish mathematician, was the first who discovered period-doubling cascades for periodic orbits with periods $p \times 2^q$, $q = 1,2,3, \ldots$, for a variety of p values in a series of articles published in 1958–1963 (46,47), reviewed in (35). In the late 1970s, Mitchell J. Feigenbaum discovered a remarkable universality for the period-doubling bifurcation cascades in 1D iterated maps (33). Specifically, Feigenbaum discovered that if d_k is defined by $d_k = p_{k+1} - p_k$, where p_k is the given map's bifurcation parameter value corresponding to the k-th period doubling bifurcation with the period transition $2^k \to 2^{k+1}$, then

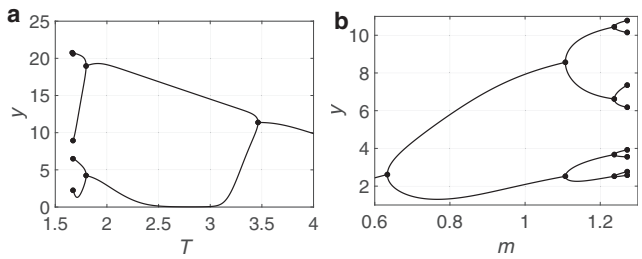

FIGURE 4 (*a* and *b*) A Feigenbaum period-doubling tree. Because of the very fast accumulation of the bifurcation values of the corresponding parameters, T_k and m_k ($k = 1, 2,\ldots$), around their respective limits (Table 1), only the very well-visible onsets of the bifurcation trees are shown.

$$\delta = \lim_{k\to\infty} \frac{d_k}{d_{k+1}} = 4.669202\ldots. \qquad (6)$$

The number δ, known as the "Feigenbaum constant", is as fundamental a quantity as the numbers π and e, in that it appears throughout the realms of science. The constant δ can be found not only in iterative maps but also in certain differential equations, for example, in the Duffing equation, as empirically shown in (34). We next check if the corresponding bifurcation values of the parameters T and m also satisfy the universality law (6).

To carry out the corresponding computations systematically, we employed the command-line version of MatcontM (38). Specifically, we used MatcontM to compute the Feigenbaum (bifurcation) tree (Fig. 4), leading to the rapid accumulation of regular saddle periodic points which eventually form an infinite countable set around the parameter value T^* (Fig. 4 *a*), or m^* (Fig. 4 *b*), correspondingly.

Here, T^* (or m^*) corresponds to the Feigenbaum constant in the limit, $T_k \to T^*$ (or $m_k \to m^*$) and $\delta_k \to \delta$, as $k \to \infty$ (Table 1).

TABLE 1 Numerical Approximation of the Feigenbaum Constant δ

k	T_k	δ_k	m_k	δ_k
1	3.46269	–	0.63353	–
2	1.79848	–	1.10720	–
3	1.67155	13.11112	1.23735	3.63917
4	1.66440	17.74194	1.27174	3.78548
5	1.66345	7.52016	1.27984	4.24533
6	1.66326	5.13666	1.28161	4.55884
7	1.66322	4.72916	1.28200	4.64452

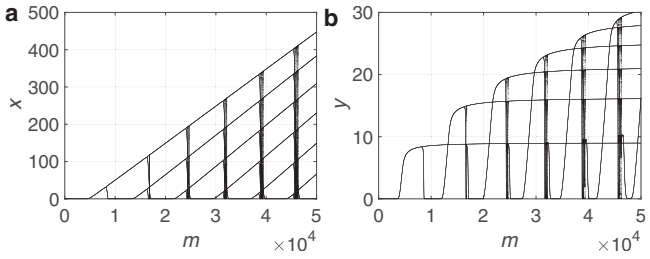

FIGURE 5 (*a* and *b*) Multiple cascades in the unity model with respect to input strength m at $T = 100$.

We find from Table 1 that whereas the sequence $\{T_k\}$ converges slowly, the sequence $\{m_k\}$ converges rapidly to its limit and its rate of convergence approximates the Feigenbaum constant very well.

Multiple cascades

We next proceed with the discussion of the bifurcation diagrams shown in Fig. 2, *c* and *d*. Specifically, we discuss the intervals in the values of the parameter T with chaotic and regular dynamics interchange, as can be observed from Fig. 2, *c* and *d*. A similar phenomenon holds for the bifurcations with respect to the parameter m characterizing the input strength (Fig. 5).

The behavior of the unity model turned out to be so complex that it was impossible to employ MatcontM to carry out a detailed numerical bifurcation analysis similarly to that completed for model 1, and discussed in the Supporting Material. Despite the complexity of the observed dynamics (Figs. 2, *c* and *d*, and 5), we emphasize here that this model is exactly the type of very complex dynamical system for which the theory developed in (35) can be applied to attain insight into the origin of the model's chaotic behavior. Due to the theory (35) and our numerical evidence, we have a strong belief that multiple period-doubling cascades contribute to the formation of the corresponding strange attractors in these cases. Such multiple cascades lead to the formation of an infinite countable set of saddle periodic points that give rise to the emergence of chaos (35).

Unbounded chaos

We complete our discussion of chaos emerging in these simple periodically forced models with the case in which model 2 has a strange attractor that appears to exist for unbounded values of the bifurcation parameter m as verified in our intensive numerical computations (Fig. 6).

We observe from Fig. 6 that although the magnitude of chaotic changes in the y variable stays bounded as in Fig. 6 *b*, the magnitude of chaotic changes in the x variable grows monotonically as the values of the bifurcation parameter m increase as in Fig. 6 *a*. The complex dynamics within such strange attractors is called "unbounded chaos" (35). Moreover, the theory predicts the existence of a cascade leading to the formation of strange attractors with unbounded chaos (35).

Effect of noise

We now briefly explore the effect of additive noise by studying the Itô stochastic differential equation (SDE):

$$dX = \left(\frac{\sigma_x u(t)}{\theta_y + Y} - \frac{\mu_x X}{M_x + X}\right) dt + \varepsilon_1 \, dW_X, \qquad (7a)$$

$$dY = \left(\frac{\sigma_y X}{\theta_x + X} - \frac{\mu_y Y}{M_y + Y}\right) dt + \varepsilon_2 \, dW_Y. \qquad (7b)$$

In the SDE given in Eqs. 7a and 7b, the parameters ${\varepsilon_1}^2$ and ${\varepsilon_2}^2$ describe the variance rates for the changes in the net rates of the random variables X and Y, respectively. Recall that the stochastic differentials dW_X and dW_Y describe the standard Winner process (the standard Brownian motion) (48,49). We write the SDE using a full differential form because W_X and W_Y are nowhere differentiable with probability one (48,50), and we solve the SDE numerically using the Milstein scheme (50,51) implemented in the MATLAB SDE Toolbox (52).

The results of numerical simulation of the SDE for different noise levels are shown in Fig. 7 for the set of

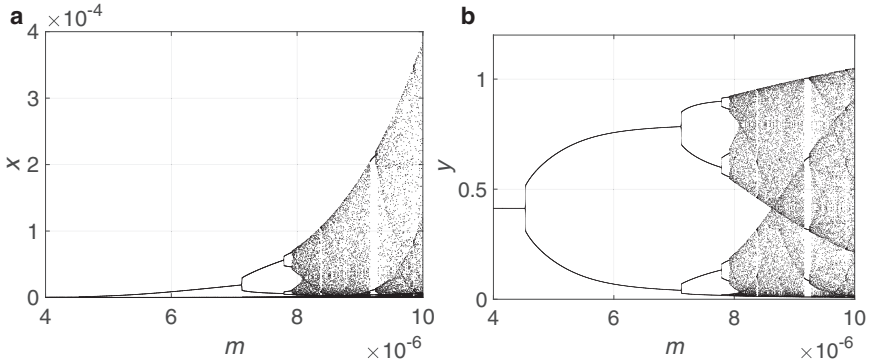

FIGURE 6 (*a* and *b*) Unbounded chaos cascade in model 2 with respect to input strength m at $T = 5$.

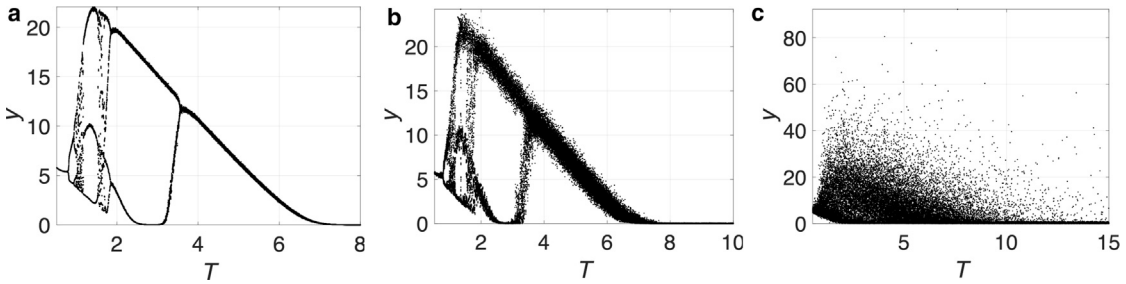

FIGURE 7 Bifurcation diagrams with respect to the external period T in the presence of noise (unity model 1). Here, (a–c) correspond, respectively, to the noise levels $\varepsilon_2 = 0.01$, $\varepsilon_2 = 0.1$, and $\varepsilon_2 = 1.0$ taken from Eqs. 7a and 7b. In all cases, $\varepsilon_1 = 10^{-6}$. The deterministic parameter values are as used in Fig. 2, a and b.

parameter values corresponding to model 1, and in Fig. 8 for the set of parameter values corresponding to the unity model. In each case, five traces or, equivalently, five stochastic trajectories starting from the same initial conditions are computed and used to plot the corresponding stochastic bifurcation diagrams.

We observe that for the smallest variance (the noise level $\varepsilon_2 = 0.01$ in Figs. 7 a and 8, a and b), the stochastic bifurcation diagrams are similar to the corresponding fully deterministic bifurcation diagrams shown in Fig. 2. For the medium-valued variance (the noise level $\varepsilon_2 = 0.1$ in Fig. 7 b), the structure of deterministic bifurcation diagrams is preserved, although large numerical clouds become clearly visible. For the larger values of the variance (the noise level $\varepsilon_2 = 1.0$ in Fig. 7 c, and $\varepsilon_2 = 0.1$ in Fig. 8, c and d), the structure of the corresponding deterministic bifurcation diagrams is destroyed. If the values of the variances are further increased, the deterministic strange attractors disappear at the cost of stability loss.

CONCLUSIONS

We showed that simple biochemical systems commonly seen in models of sensing and signal transduction pathways are able to exhibit a rich bifurcation structure into subharmonic oscillations, and even chaotic behavior, in response to periodic excitations.

The appearance of subharmonic responses is by no means an automatic property of cellular biochemical systems, however. For example, models of processes involved in gene transcription (53) and mRNA translation (54) can be shown to display the opposite behavior, namely entrainment, which means that all solutions have the same frequency as the forcing periodic signal. More generally, the synchronization of

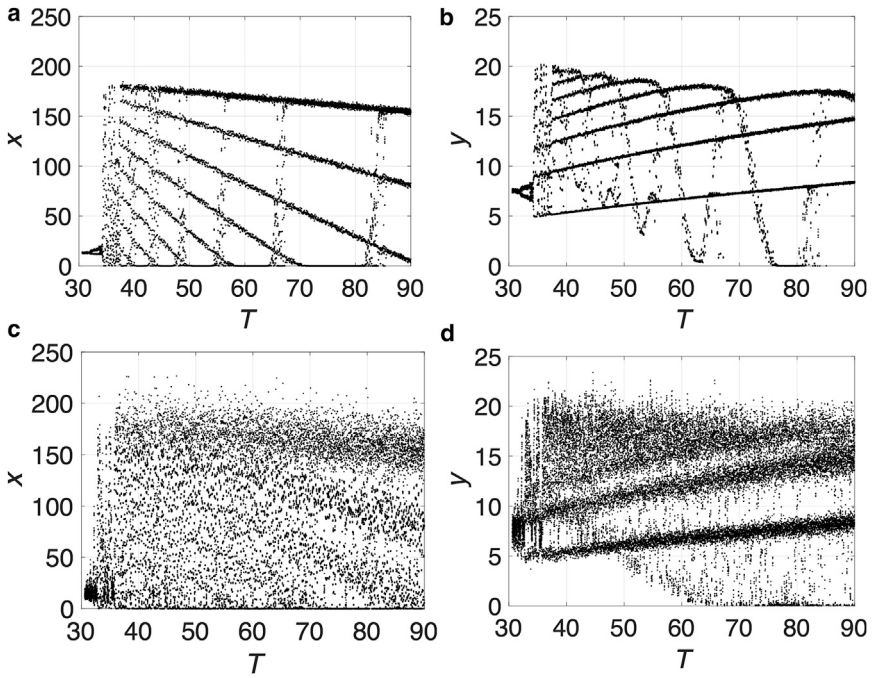

FIGURE 8 Bifurcation diagrams with respect to the external period T in the presence of noise (unity model 1). Here, (a) and (b) correspond to the noise level $\varepsilon_2 = 0.01$ taken from Eqs. 7a and 7b; and (c) and (d) correspond to the noise level $\varepsilon_2 = 0.1$ taken from Eqs. 7a and 7b. In all cases, $\varepsilon_1 = 10^{-6}$. The deterministic parameter values are as used in Fig. 2, c and d.

oscillators to external signals whose magnitude is large enough to enter the "Arnold tongue" insures that solutions will have the same frequency as the input (55). As pointed out in a recent article (56), entrained responses of biological systems play a key regulatory role in organisms (57–59).

Although the behavior that we uncovered theoretically is consistent with the nonentrained responses seen experimentally in (14), it is virtually impossible to mathematically prove that an experimentally observed behavior is chaotic, or even perfectly subharmonic, especially in molecular biology, where noisy and relatively low precision measurements are the rule. Nonetheless, this work can serve as an indication that a lack of entrainment, complicated bifurcation structure, and chaotic behavior even in some of the simplest biochemical models, need not necessarily appeal to randomness or complex hidden regulatory pathways.

SUPPORTING MATERIAL

Supporting Materials and Methods and eight figures are available at http://www.biophysj.org/biophysj/supplemental/S0006-3495(18)30071-7.

AUTHOR CONTRIBUTIONS

E.D.S. and S.J.R. conceived the work. E.V.N. and E.D.S. designed research. E.V.N. performed research and analyzed data. S.J.R. contributed data. E.V.N. and E.D.S. wrote the manuscript.

ACKNOWLEDGMENTS

This research was supported in part by grant Air Force Office of Scientific Research FA9550-14-1-0060 and grant Office of Naval Research N00014-13-1-0074.

REFERENCES

1. Ferrell, J. E., Jr. 2002. Self-perpetuating states in signal transduction: positive feedback, double-negative feedback and bistability. *Curr. Opin. Cell Biol.* 14:140–148.
2. Tyson, J. J., K. C. Chen, and B. Novak. 2003. Sniffers, buzzers, toggles and blinkers: dynamics of regulatory and signaling pathways in the cell. *Curr. Opin. Cell Biol.* 15:221–231.
3. Pomerening, J. R., E. D. Sontag, and J. E. Ferrell, Jr. 2003. Building a cell cycle oscillator: hysteresis and bistability in the activation of Cdc2. *Nat. Cell Biol.* 5:346–351.
4. Markevich, N. I., J. B. Hoek, and B. N. Kholodenko. 2004. Signaling switches and bistability arising from multisite phosphorylation in protein kinase cascades. *J. Cell Biol.* 164:353–359.
5. Craciun, G., Y. Tang, and M. Feinberg. 2006. Understanding bistability in complex enzyme-driven reaction networks. *Proc. Natl. Acad. Sci. USA.* 103:8697–8702.
6. Thomson, M., and J. Gunawardena. 2009. Unlimited multistability in multisite phosphorylation systems. *Nature.* 460:274–277.
7. Wang, L., and E. D. Sontag. 2008. On the number of steady states in a multiple futile cycle. *J. Math. Biol.* 57:29–52.
8. Siegal-Gaskins, D., E. Grotewold, and G. D. Smith. 2009. The capacity for multistability in small gene regulatory networks. *BMC Syst. Biol.* 3:96.
9. Thomas, R. 1981. On the Relation Between the Logical Structure of Systems and Their Ability to Generate Multiple Steady States or Sustained Oscillations. Springer, Berlin, Germany, pp. 180–193.
10. Shoval, O., L. Goentoro, …, U. Alon. 2010. Fold-change detection and scalar symmetry of sensory input fields. *Proc. Natl. Acad. Sci. USA.* 107:15995–16000.
11. Lazova, M. D., T. Ahmed, …, T. S. Shimizu. 2011. Response rescaling in bacterial chemotaxis. *Proc. Natl. Acad. Sci. USA.* 108:13870–13875.
12. Hamadeh, A., B. Ingalls, and E. Sontag. 2013. Transient dynamic phenotypes as criteria for model discrimination: fold-change detection in *Rhodobacter sphaeroides* chemotaxis. *J. R. Soc. Interface.* 10: 20120935.
13. Ascensao, J. A., P. Datta, …, O. A. Igoshin. 2016. Non-monotonic response to monotonic stimulus: regulation of glyoxylate shunt gene-expression dynamics in *Mycobacterium tuberculosis*. *PLoS Comput. Biol.* 12:e1004741.
14. Rahi, S. J., J. Larsch, …, F. R. Cross. 2017. Oscillatory stimuli differentiate adapting circuit topologies. *Nat. Methods.* 14:1010–1016.
15. Matsumoto, G., K. Aihara, …, J. -i. Nagumo. 1987. Chaos and phase locking in normal squid axons. *Phys. Lett. A.* 123:162–166.
16. Goldbeter, A., D. Gonze, …, G. Dupont. 2001. From simple to complex oscillatory behavior in metabolic and genetic control networks. *Chaos.* 11:247–260.
17. Duffing, G. 1918. Erzwungene Schwingungen bei Veränderlicher Eigenfrequenz und ihre Technische Bedeutung. Vieweg & Sohn, Berlin, Germany.
18. Wiggins, S. 1987. Chaos in the quasiperiodically forced duffing oscillator. *Phys. Lett. A.* 124:138–142.
19. Rajasekar, S., and M. Lakshmanan. 1988. Period doubling route to chaos for a BVP oscillator with periodic external force. *J. Theor. Biol.* 133:473–477.
20. Ueda, Y., R. H. Abraham, and H. B. Stewart. 2001. The Road to Chaos. Aerial Press, New Orleans, LA.
21. Abraham, R. H., and Y. Ueda. 2001. The Chaos Avant-Garde: Memories of the Early Days of Chaos TheoryVol. 39. World Scientific, Singapore.
22. Guckenheimer, J., and P. J. Holmes. 2013. Nonlinear Oscillations, Dynamical Systems, and Bifurcations of Vector FieldsVol. 42. Springer Science & Business Media, Berlin, Germany.
23. Holmes, P. 2005. Ninety plus thirty years of nonlinear dynamics: less is more and more is different. *Int. J. Bifurcat. Chaos.* 15:2703–2716.
24. Tomita, K., and T. Kai. 1978. Stroboscopic phase portrait and strange attractors. *Phys. Lett. A.* 66:91–93.
25. Itō, A. 1979. Perturbation theory of self-oscillating system with a periodic perturbation. *Prog. Theor. Phys.* 61:45.
26. Shoval, O., U. Alon, and E. D. Sontag. 2011. Symmetry invariance for adapting biological systems. *SIAM J. Appl. Dyn. Syst.* 10:857–886.
27. Afraimovich, V. S., V. I. Arnold, …, L. P. Shilnikov. 1989. Dynamical Systems V. Encyclopedia of Mathematical Sciences. Springer, Heidelberg, Germany..
28. Kuznetsov, Y. A., S. Muratori, and S. Rinaldi. 1992. Bifurcations and chaos in a periodic predator-prey model. *Int. J. Bifurcat. Chaos.* 2:117–128.
29. Shilnikov, L. P., A. L. Shilnikov, …, L. O. Chua. 1998. Methods of Qualitative Theory in Nonlinear Dynamics. World Scientific, Singapore.
30. Guckenheimer, J., M. Wechselberger, and L.-S. Young. 2006. Chaotic attractors of relaxation oscillators. *Nonlinearity.* 19:701.
31. Anishchenko, V. S., V. Astakhov, …, L. Schimansky-Geier. 2007. Nonlinear Dynamics of Chaotic and Stochastic Systems: Tutorial and Modern Developments. Springer Science & Business Media, Berlin, Germany.
32. Wiggins, S. 2013. Global Bifurcations and Chaos: Analytical MethodsVol. 73. Springer Science & Business Media, Berlin, Germany.

33. Feigenbaum, M. J. 1979. The universal metric properties of nonlinear transformations. *J. Stat. Phys.* 21:669–706.
34. Feigenbaum, M. J. 1983. Universal behavior in nonlinear systems. *Physica D.* 7:16–39.
35. Sander, E., and J. A. Yorke. 2013. A period-doubling cascade precedes chaos for planar maps. *Chaos.* 23:033113.
36. Holmes, P. 1979. A nonlinear oscillator with a strange attractor. *Phil. Trans. R. Soc. Lond. A.* 292:419–448.
37. Khibnik, A. I., Y. A. Kuznetsov, …, E. V. Nikolaev. 1993. Continuation techniques and interactive software for bifurcation analysis of ODEs and iterated maps. *Physica D.* 62:360–371.
38. Neirynck, N., B. Al-Hdaibat, …, H. G. E. Meijer. 2016. Using MatContM in the study of a nonlinear map in economics. *J. Phys. Conf. Ser.* 692:012013.
39. Bogoliubov, N. N., and Y. A. Mitropolsky. 1961. Asymptotic Methods in the Theory of Non-Linear Oscillations. Hindustan Publishing Corporation, Delhi, India.
40. Bogoliubov, N. N., Y. A. Mitropolsky, and J. Gillis. 1963. Asymptotic methods in the theory of non-linear oscillations. *Phys. Today.* 16:61.
41. Nikolaev, E. V., J. C. Atlas, and M. L. Shuler. 2007. Sensitivity and control analysis of periodically forced reaction networks using the Green's function method. *J. Theor. Biol.* 247:442–461.
42. Wolf, A., J. B. Swift, …, J. A. Vastano. 1985. Determining Lyapunov exponents from a time series. *Physica D.* 16:285–317.
43. Melbourne, I., and G. A. Gottwald. 2007. Power spectra for deterministic chaotic dynamical systems. *Nonlinearity.* 21:179.
44. Dunn, P. F. 2014. Measurement and Data Analysis for Engineering and Science. CRC Press, Boca Raton, FL.
45. Marchesoni, F. 1994. Nucleation of kinks in 1+1 dimensions. *Phys. Rev. Lett.* 73:2394–2397.
46. Myrberg, P. J. 1962. Sur l'itération des polynomes réels quadratiques. *J. Math. Pures Appl.* 41:339–351.
47. Myrberg, P. J. 1963. Iteration der reellen polynome zweiten grades III. *Ann. Acad. Sci. Fenn. [Biol.].* 336:1.
48. Higham, D. J. 2001. An algorithmic introduction to numerical simulation of stochastic differential equations. *SIAM Rev.* 43:525–546.
49. Allen, L. J. S. 2010. An Introduction to Stochastic Processes with Applications to Biology. CRC Press, Boca Raton, FL.
50. Evans, L. C. 2012. An Introduction to Stochastic Differential EquationsVol. 82. American Mathematical Society, Providence, RI.
51. Higham, D. J. 2008. Modeling and simulating chemical reactions. *SIAM Rev.* 50:347–368.
52. Picchini, U. 2007. SDE toolbox: simulation and estimation of stochastic differential equations with MATLAB. http://www.maths.lth.se/matstat/staff/umberto.
53. Russo, G., M. di Bernardo, and E. D. Sontag. 2010. Global entrainment of transcriptional systems to periodic inputs. *PLoS Comput. Biol.* 6:e1000739.
54. Margaliot, M., E. D. Sontag, and T. Tuller. 2014. Entrainment to periodic initiation and transition rates in a computational model for gene translation. *PLoS One.* 9:e96039.
55. Pikovsky, A., M. Rosenblum, and J. Kurths. 2001. Synchronization: A Universal Concept in Nonlinear Sciences. Cambridge University Press, Cambridge, United Kingdom.
56. Gupta, A., B. Hepp, and M. Khammash. 2016. Noise induces the population-level entrainment of incoherent, uncoupled intracellular oscillators. *Cell Syst.* 3:521–531.e13.
57. Han, Q., N. Bagheri, …, J. C. Love. 2012. Polyfunctional responses by human T cells result from sequential release of cytokines. *Proc. Natl. Acad. Sci. USA.* 109:1607–1612.
58. Kalsbeek, A., S. la Fleur, and E. Fliers. 2014. Circadian control of glucose metabolism. *Mol. Metab.* 3:372–383.
59. Lin, Y., C. H. Sohn, …, M. B. Elowitz. 2015. Combinatorial gene regulation by modulation of relative pulse timing. *Nature.* 527:54–58.

Biophysical Journal, Volume *114*

Supplemental Information

Subharmonics and Chaos in Simple Periodically Forced Biomolecular Models

Evgeni V. Nikolaev, Sahand Jamal Rahi, and Eduardo D. Sontag

SI-1 Global dynamics of the model (1) with constant imputs

Consider the system described by (1), with a constant input $u(t) \equiv u_0$:

$$F(x,y) = \frac{\sigma_x u_0}{\theta_y + y} - \frac{\mu_x x}{M_x + x} \tag{SI-1.1a}$$

$$G(x,y) = \frac{\sigma_y x}{\theta_x + x} - \frac{\mu_y y}{M_y + y}. \tag{SI-1.1b}$$

We first note that a steady state, if it exists, is unique (clearly because of the increasing or decreasing character of the functions of x and y). An analysis of nullclines reveals that there is only one case in which solutions may become unbounded, see Figure SI-1.1, and our examples never treat that case.

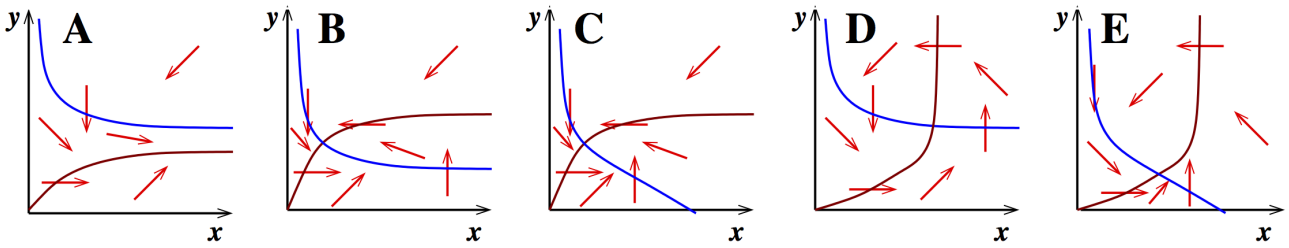

Figure SI-1.1: Possible phase planes. The blue curve represents the x-nullcline, that is, the locus of $\frac{\sigma_x u_0}{\theta_y+y} = \frac{\mu_x x}{M_x+x}$, and the brown curve represents the y-nullcline, that is, the locus of $\frac{\mu_y y}{M_y+y} = \frac{\sigma_y x}{\theta_x+x}$. Arrows indicate directions of movement. In cases B-E, solutions remain bounded. In case A, solutions may diverge. Case A occurs when both of the following conditions hold: (i) $\mu_y > \sigma_y$ and (ii) $\sigma_y M_y/(\mu_y - \sigma_y) < (\sigma_x u_0/\mu_x) - \theta_y$. (These conditions characterize that case when both nullclines have have a positive limit as $x \to \infty$, and they do not cross.) Note that we picked up the parameter values so that (i) fails: $\mu_y = 10$, $\sigma_y = 10^4$ (or both equal to 1 in the "unity" model).

Once that boundedness if the solutions is established, the Poincaré-Bendixson Theorem [1] insures that every solution converges to the unique equilibrium, unless there are periodic solutions or heteroclinic (including homoclinic) connections. However, periodic solutions and connections are ruled out by the Bendixson criterion [1], as follows. Consider the vector field $V(x,y) = (F(x,y), G(x,y))$, corresponding to the model in equations (SI-1.1). The Bendixson's criterion states that if $\mathrm{div} V(x,y) \neq 0$ for all $(x,y) \in D$, then the vector field $V(x,y)$ does not have a closed orbit or heteroclinic connections in D, where D is any simply connected region of $\mathbb{R}^2$, $D \subseteq \mathbb{R}^2$, and

$$\mathrm{div}\,(V(x,y)) = \frac{\partial F(x,y)}{\partial x} + \frac{\partial G(x,y)}{\partial y}. \tag{SI-1.2}$$

To show that $\mathrm{div} V(x,y) \neq 0$, $\forall\,(x,y) \in D = \mathbb{R}^2$, we simply compute:

$$\mathrm{div}\,(V(x,y)) = -\left(\frac{\mu_x M_x}{(M_x + x)^2} + \frac{\mu_y M_y}{(M_y + y)^2}\right) < 0, \qquad \forall\,(x,y) \in \mathbb{R}^2. \tag{SI-1.3}$$

SI-2 Numerical evaluation of largest Lyapunov exponents

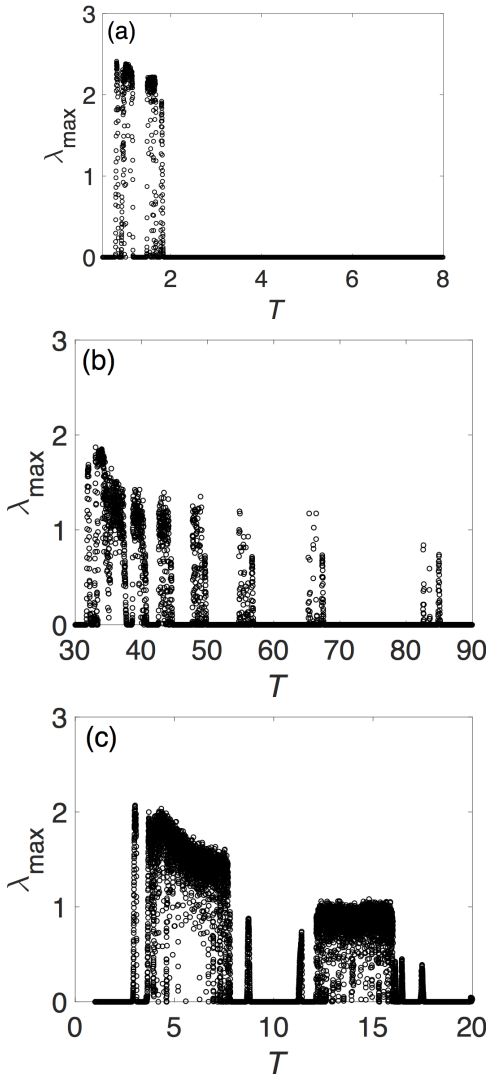

Figure SI-2.1: Largest Lyapunov exponents λ_{max} depending on external period T. Panel (a) corresponds to panels (a) and (b) from Fig. 2 in the main text; panel (b) corresponds to panels (c) and (d) from Fig. 2; and panel (c) corresponds to panels (e) and (f) from Fig. 2. Positive values $\lambda_{max} > 0$ characterize chaotic solutions, while zero values, $\lambda_{max} = 0$, are associated with periodic solutions of the corresponding models with the parameter values given in Sect. 3 of the main text.

SI-3 Examples of chaotic solutions

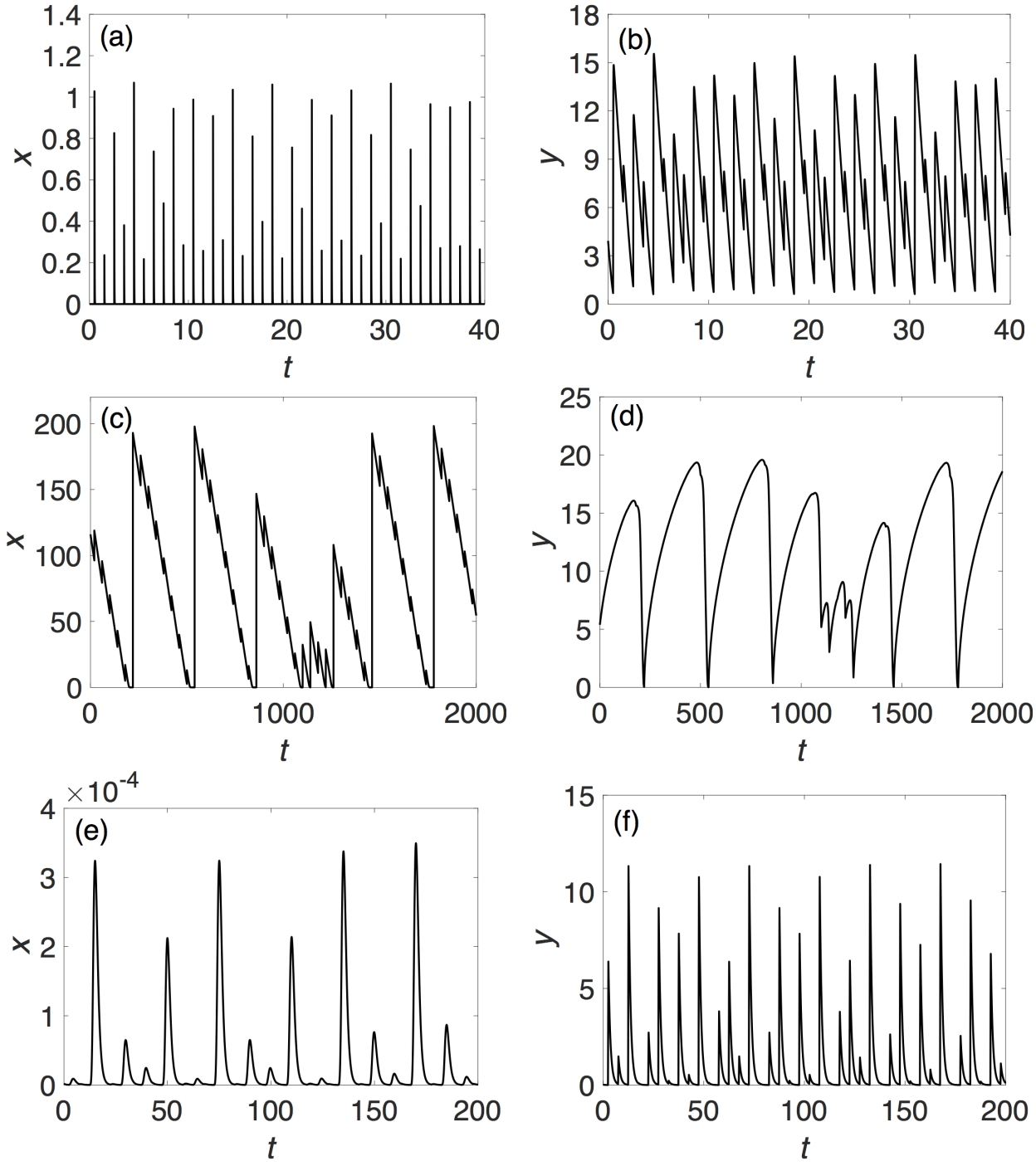

Figure SI-3.1: Chaotic solutions. Panels (a) and (b) correspond to model (1) with $T = 1.0$ and $\lambda_{\max} \approx 1.97$; panels (c) and (d) correspond to the unity model with $T = 40$ and $\lambda_{\max} \approx 0.86$; and panels (e) and (f) correspond to model (2) with $T = 5$ and $\lambda_{\max} \approx 0.82$. All other fixed parameter values are given in Sect. 3. In panel (a), $x(t)$ decays extremely fast, hence the "spike" look of the plot.

SI-4 Scatter plots and marginal distributions

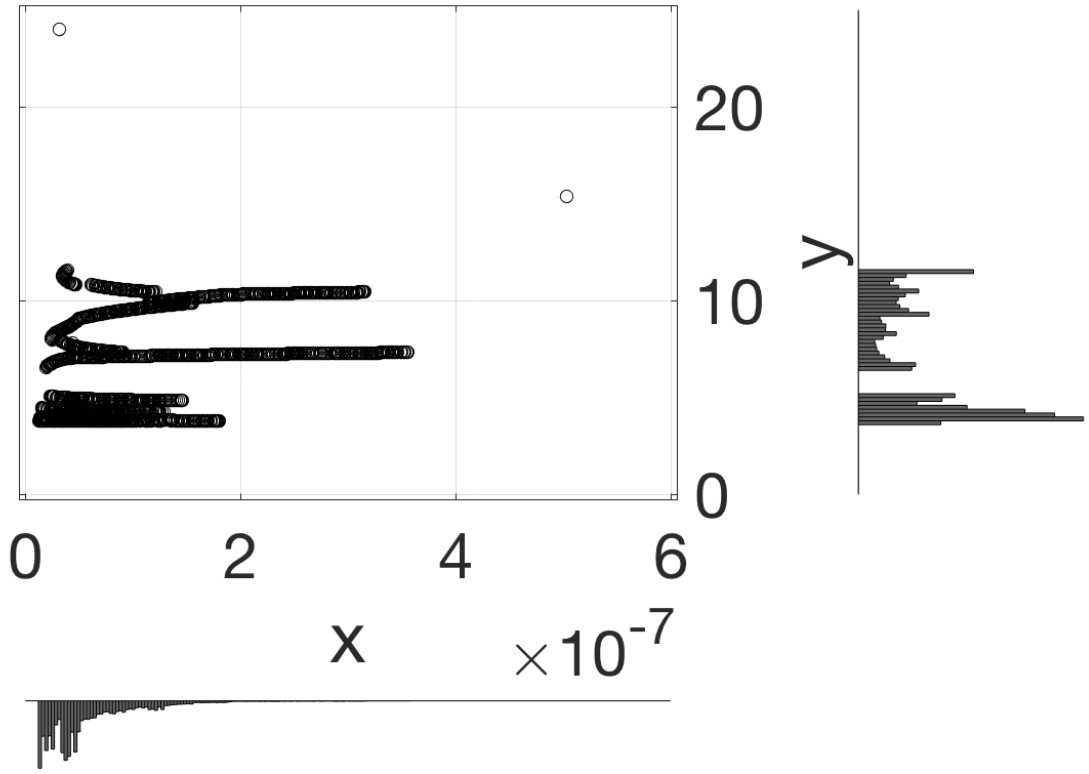

Figure SI-4.1: Scatter plot and marginal distributions for the model (1) with period $T = 1$.

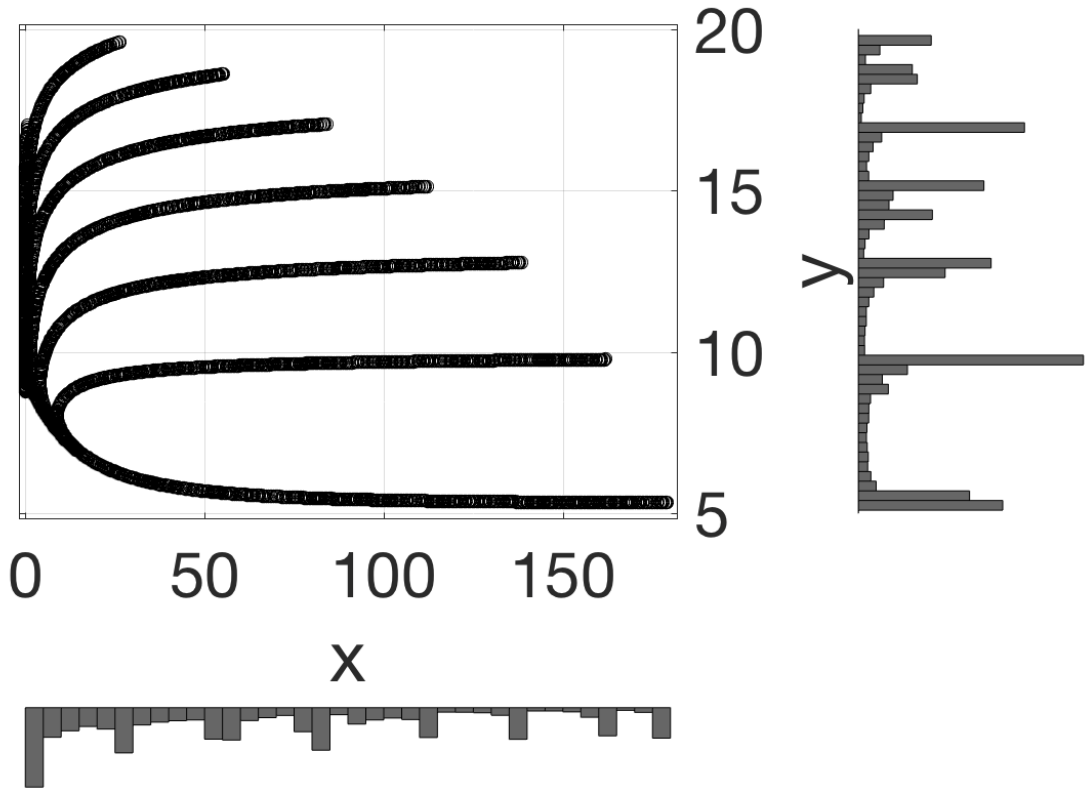

Figure SI-4.2: Scatter plot and marginal distributions for the unity model (1) with period $T = 40$.

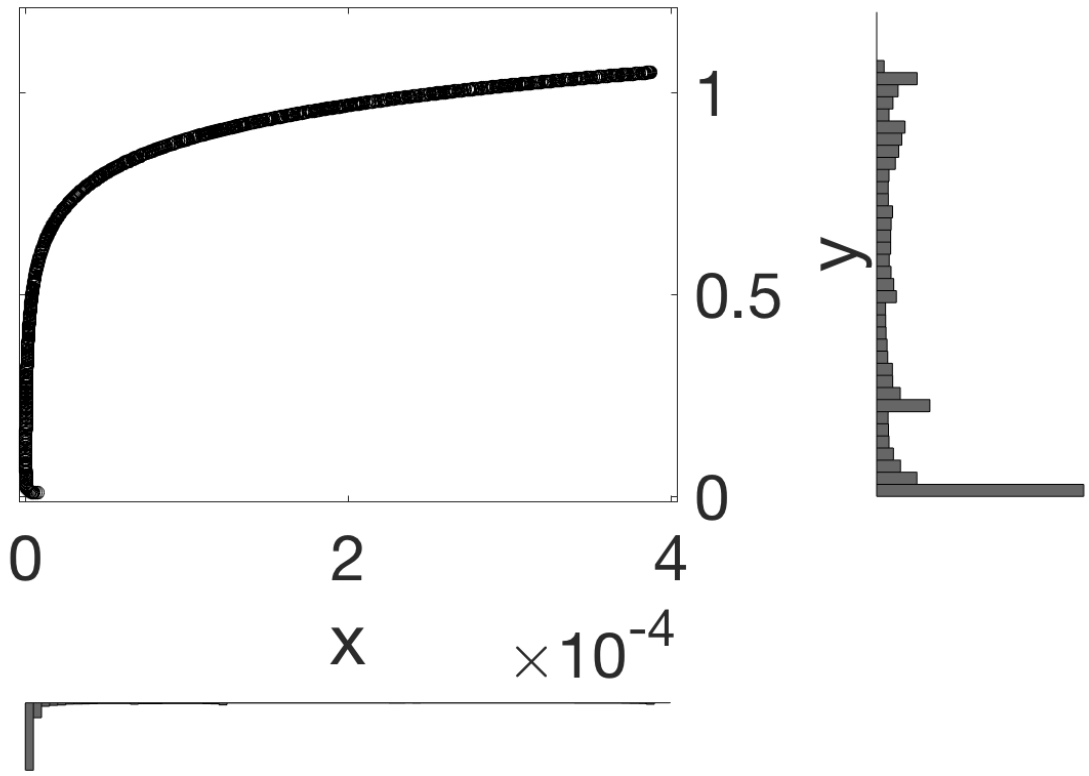

Figure SI-4.3: Scatter plot and marginal distributions for the FCD model (2) with period $T = 5$.

SI-5 Bifurcation diagrams with respect to the input signal support Δ

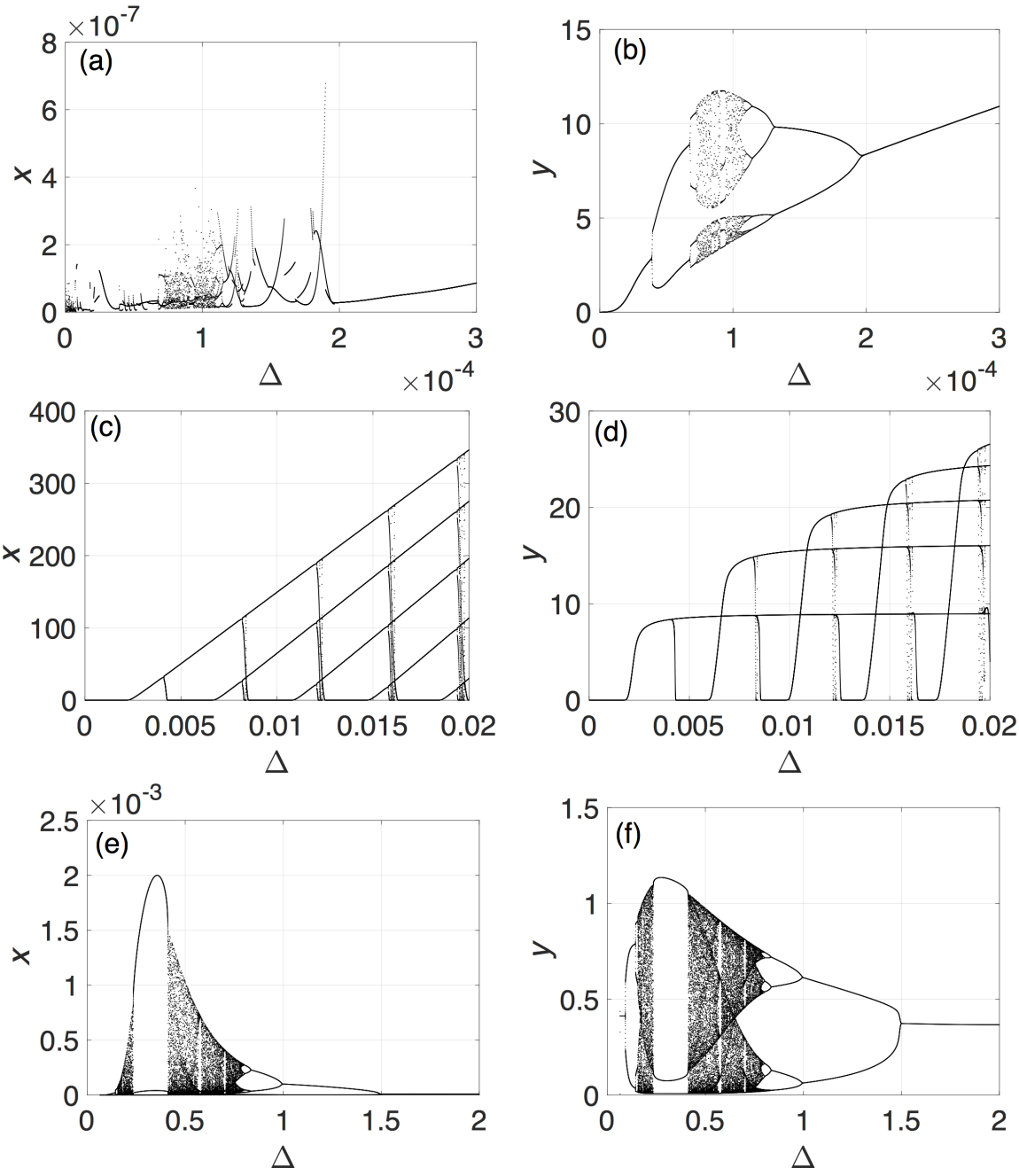

Figure SI-5.1: Bifurcation diagrams with respect to the input signal support Δ. Panels (a) and (b) correspond to model (1) with $T = 1$; panels (c) and (d) correspond to the unity model (1) with $T = 100$; and panels (e) and (f) correspond to model (2) with $T = 5$.

SI-6 Experimental results

In [2], experiments were performed on intact *C. elegans* worms in microfluidic chambers, measuring the response of odor-sensing AWA neurons (quantified by intracellular Ca^{2+} activity as measured by an AWA-specific GCaMP sensor) to periodic on-off pulses of diacetyl. Shown in Fig. SI-6.1 is a harmonic response in one experiment to a pulse with period $T = 39$, as well as, for another experiment, what looks like sub-harmonic responses when the period of pulses is shorter, $T = 15$. (Not shown are preparatory odor pulses, used in order to calibrate the recordings across experiments by waiting for stabilized responses.) The experiments used the technology developed in [2].

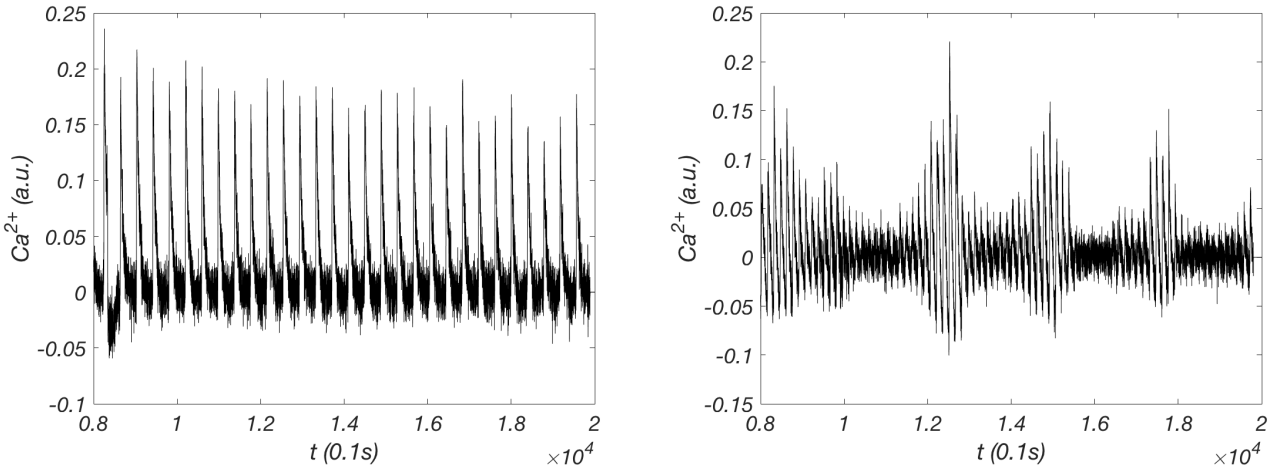

Figure SI-6.1: Two selected responses to longer and shorter periods, from the work [2]. The x-axis represents time in units of 0.1 seconds, and the y-axis is intracellular Ca^{2+} activity in arbitrary units. Top: A trace showing an approximately harmonic (entrained) response to a pulse train with period $T = 39$s. Bottom: A trace showing a non-entrained response, with an apparent lower-frequency component, to a pulse train with period $T = 15$s. Pulse duration $\Delta = 10$s in both cases. See [2] for details.

SI-7 Verification of smoothness of $\Phi(z, \alpha)$

We wish to prove that $\Phi(z, \alpha)$ is smooth, for our models with the piecewise defined input (3). The result follows from a general theorem on the smooth dependence of the solutions of the given ODE on initial conditions and parameters, see e.g. [3]. Indeed, let us first represent $\Phi(z, \alpha)$ in the following superposition form,

$$\Phi(z, \alpha) \, = \, \varphi^{T-t_2} \circ \varphi^{t_2-t_1} \circ \varphi^{t_1}(z, \alpha). \tag{SI-7.1}$$

Let $z_1(z, \alpha) \, = \, \varphi^{t_1}(z, \alpha)$, $z_2(z_1, \alpha) \, = \, \varphi^{t_2-t_1}(z_1, \alpha)$, and $z_3(z_2, \alpha) = \varphi^{T-t_2}(z_2, \alpha)$.

Since $z_1(z, \alpha)$ smoothly depends on z, $z_2(z_1)$ smoothly depends on z_1 (viewed as an independent initial condition), and, analogously, $z_3(z_2, \alpha)$ smoothly depends on z_2, it follows from the differentiation chain rule applied to the superposition (SI-7.1) that $\Phi(z, \alpha)$ smoothly depends on the state variable z [3].

Similarly, because each of the shift maps, $\varphi^{T-t_2}(z_2, \alpha)$, $\varphi^{t_2-t_1}(z_1, \alpha)$, and $\varphi^{t_1}(z, \alpha)$, smoothly depends on the parameter α, we can conclude that $\Phi(z, \alpha)$ as well smoothly depends on the parameter α [3].

Moreover, it can be proved that $\Phi(z, \alpha)$ is a diffeomorphism [3].

SI-8 Tuning parameters of MatcontM

To clarify our computational approach, we have to note that the default setup of MatcontM implicitly requires that the map $\Phi(z, \alpha)$ is given by explicit analytic expressions (formulas), since it uses algorithmic differentiation to compute Poincaré normal form coefficients [4]. Because our map $\Phi(z, \alpha)$ is defined implicitly through a number of numerical integration steps, we disabled the algorithmic (also called automatic or symbolic) differentiation (`adtayl`) feature by setting '`AutDerivative`' = 0.

To ensure robustness of all numerical computations, we used the MATLAB© ode45, ode15s, and ode23s solvers with tight values of '`RelTol`' = 10^{-8} and '`AbsTol`' = 10^{-10}, and, additionally, with '`RelTol`' = 10^{-10} and '`AbsTol`' = 10^{-12}. To obtain all bifurcation values of both T_k and m_k with at least five significant digits, we computed the corresponding values two times by setting (*i*) '`FunTolerance`' = 10^{-6} and 10^{-8}, (*ii*) '`VarTolerance`' = 10^{-6} and 10^{-8}, and (*iii*) '`TestTolerance`' = 10^{-5} and 10^{-7} inside MatcontM.

References

[1] S. Wiggins. *Introduction to applied nonlinear dynamical systems and chaos*, volume 2. Springer Science & Business Media, 2003.

[2] S. J. Rahi, J. Larsch, K. Pecani, A. Y. Katsov, N. Mansouri, K. Tsaneva-Atanasova, E. D. Sontag, and F. R. Cross. Oscillatory stimuli differentiate adapting circuit topologies. *Nat. Methods*, 14(10):1010–1016, Oct 2017.

[3] E. D. Sontag. *Mathematical control theory: deterministic finite dimensional systems*, volume 6. Springer, 2013.

[4] J. D. Pryce, R. K. Ghaziani, V. De Witte, and W. Govaerts. Computation of normal form coefficients of cycle bifurcations of maps by algorithmic differentiation. *Mathematics and Computers in Simulation*, 81(1):109–119, 2010.